Fabrication and Characterization of Li-6 Sandwich Detector

Kiwhan Chung[a*], Metodi Iliev[b], Kiril Ianakiev[b], Martyn Swinhoe[b]

[a]Future & Challenge Technology Co., Ltd., Heungdoek IT Valley Bldg, 32Fl, Heungdeok 1-ro 13,
Giheung-gu, Yongin-si, Hyeonni-do, Korea 446-902
[b]Safeguards Science & Technology, Los Alamos National Laboratory, New Mexico, USA 87544
[*]Corresponding author: kiwhan@fnctech.com

1. Introduction

Lithium-6 has been used as a radiation detector material for its ability to react with thermal neutrons, producing alphas and tritons as the primary charged particles during the neutron conversion reaction [1]. Lithium-6 has a thermal neutron cross section of 940 barns, producing a 2.05 MeV alpha particle and a 2.73 MeV triton in a back to back symmetry to conserve energy and momentum, if the incident thermal neutron has low energy [2]. The most widely recognized thermal neutron conversion reaction involves He-3. A He-3 atom has a thermal neutron cross section of 5330 barns, but its resulting particles have total 0.764 MeV to share between a proton and triton. While the conversion reaction involving lithium occurs less frequently, its resultant products stand out with higher energy output, making it a better candidate for use with scintillators. Even though lithium-6 has a high probability to interact with thermal neutrons, its highly reactive nature with moisture demands careful handling in a dry atmosphere with less than 2% humidity. Due to the access restriction put on the material by the US government and its chemical volatility, handling of the material anything but routine.

Since the terrorist attacks on September 11, 2001, the increased use of He-3 gas for neutron detection in the US decreased the stockpile of the He-3. As the He-3 is a decay product of tritium, which was produced as a part of the US nuclear weapons program in the past [3], the dwindling inventory of the He-3 is not the determining factor for its production. The use of He-3 gas is not limited to homeland security and international safeguards programs; the high energy physics and medical communities all benefit from the unique capabilities of He-3 [4].

Predicting the shortage of He-3, US government sponsors called for proposals on He-3 replacement technologies. Safeguards Science & Technology Group at the Los Alamos National Laboratory proposed using lithium-6 metal foil and has been developing neutron detectors using 95% enriched lithium-6 metal foil for homeland security and international safeguards application [5,6,7]. This lithium sandwich detector may be considered a second major iteration of the continued effort in applying lithium-6 metal foil. Fig. 1 shows the detector concept for the lithium sandwich detector. First, 5cm wide, 45cm long, 0.63 cm thick light guide strips, shown in yellow, were glued with plastic scintil-

lator film pieces, depicted in blue, on both sides. Between the light guides, a 50-micron thick lithium-6 foil, depicted in red, was placed and multiple stacks were assembled as shown in Fig. 1. Two PMTs were optically coupled to ends of light guide strips and their signals are summed to reduce light attenuation.

Fig. 1. Detector concept for the lithium sandwich detector. Li-6 metal neutron capturing foil, depicted in red, is sandwiched between scintillator films, in blue, laminated to the light guide strips. The dual side particle readout improves efficiency and pulse height distribution. The yellow body is the light guide material which transports photons to the PMTs and moderates fission neutrons.

1.1. Neutron Detection for the Lithium Sandwich Detector

Fig. 2 shows a neutron conversion scheme involving a lithium-6 atom. As fission neutrons enter the sandwich medium consisting of light guides, plastic scintillator, and lithium-6 foil, they lose energy in the volume. Some neutrons are reduced to thermal energy range and interact with lithium-6 atoms, producing a triton and an alpha particle during the reaction. The primary charged particles then impart their energies in the plastic scintillator film, producing photons. The photons then travels toward the ends of the light guide strips and get collected by the PMTs.
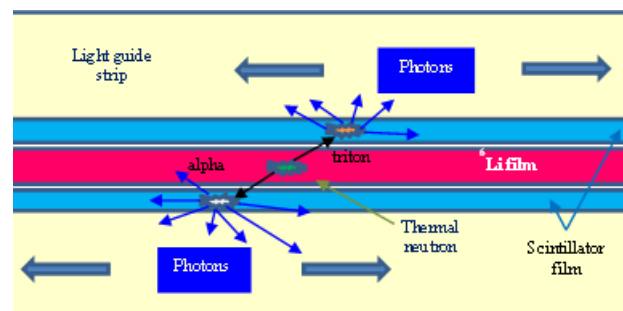
Fig. 2. A neutron conversion scheme involving a lithium-6 atom. Fission neutrons are thermalized in the multiple layers of light guide strips and react with Li-6 atoms in the foil. The primary charged particles produced from the neutron conversion reactions produce photons, which are then transported to PMTs by the light guide strips.

1.2. Li-6 Preparation

Initially, the lithium-6 metal was in storage for many years at the Y-12 National Security Complex, Oak Ridge, Tenneessee, and the metal piece needed reprocessing as shown in Fig. 3. The piece was transported to a lithium battery production facility which had the capability to reprocess lithium ingots.

Fig. 3. A piece of unprocessed lithium-6 that has been soaked in mineral oil for long-term storage at Y-12 site.

After the metal was reprocessed, it was purified to 95% enrichment and regained sheen (Fig. 4). The foil was extruded as 50-micron, 5 cm-wide strips as shown in inset of Fig. 4. The rolls were stored in an airtight pouch which was filled with dry argon and sealed in a metal container capable of withstanding long term storage as shown in Fig. 5.
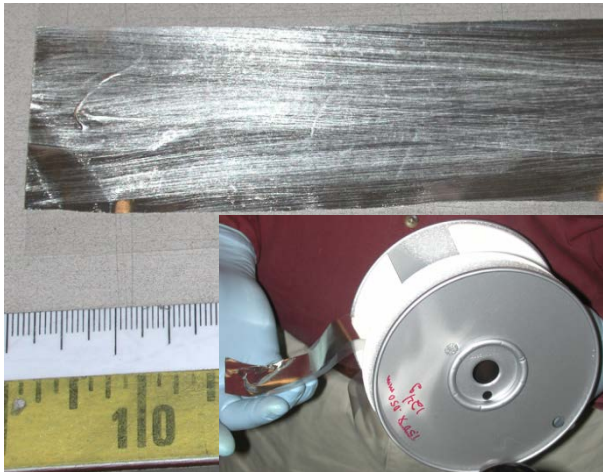
Fig. 4. The black piece in Fig. 3 is purified and refined to produce 95% enriched lithium-6 metal, which appears very similar to aluminum foil. It is packaged in 5 cm-wide rolls (shown inset) for easy handling.

When necessary, a piece of the foil was cut and applied to the metalized surface as shown in Fig. 6 [5]. Lithium can alloy with other metals, which is associated with the highly reactive nature. In case of the lithium sandwich detector, the foil was simply placed between two light guide strips laminated with plastic scintillator film on the surface.

Fig. 5. The freshly processed rolls of lithium-6 foil were then pressure packed with dry argon gas for long-term storage. The cans were pressed sealed.

Fig. 6. A piece of lithium foil is cut with a pair of scissors and pressed on to a metalized surface of a lithium-6 neutron-capture pulse mode ion chamber.

2. Component Selection

While the lithium was procured and processed, ready for fabrication, detector components were tested for characterization and optimization. The lithium foil thickness was already determined in previous studies for the optimal balance of the neutron conversion process [5,6]. The optimal lithium foil thickness is a function between neutron conversion reaction and escape probability of the primary charged particles produced. The selection of the plastic scintillator thickness, depending on gamma and charged particle responses, needed to be determined.

2.1. Scintillator Film: Heavy Charged Particle Response

Using a Pu-239 source, the detector response as a function of plastic scintillator (NE102A equivalent) thickness was obtained. Pu-239 alpha particles were chosen as an adequate substitute in the absence of 2.7 MeV triton particles. Gooding and Pugh noted that the

light output of a 3 MeV triton and a 6 MeV alpha particle was comparable in NE102 plastic scintillator film [8].

Fig. 7 shows the measurement setup for the Pu-239 alpha measurement. A 6.45 cm^2 square plastic scintillator film was cut and adhered to the face of the Hamamatsu R1307 PMT with optical grease BC-630. Then, a Pu-239 disk was taped to the plastic scintillator film, emitting alpha particles directly on to the film.
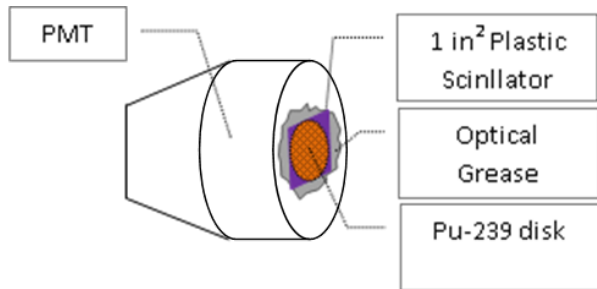
Fig. 7. The Pu-239 alpha particle measurement setup. One square-inch plastic scintillator piece was directly applied on to the PMT surface using optical grease. A Pu-239 source was taped to the scintillator for measurement.

The spectra obtained with Pu-239 alpha peaks using 50 μm BC-400 and 200 μm EJ-212 plastic scintillator films are shown in Fig. 8. Pu-239 releases alpha particles of 3 different energy levels (5.105 MeV (11.5%), 5.144 MeV (15.1%), and 5.156 MeV (73.3%)); hence, the peak has an asymmetric distribution on the left side of the peak. The BC-400 and EJ-212 films are NE-102A equivalent materials and therefore, are chemically identical. As expected, the 200 μm EJ-212 plastic scintillator film has the better energy deposition than BC-400 film. While the spectrum for 75 μm BC-400 is omitted in Fig. 8, the data were recorded in Table I.
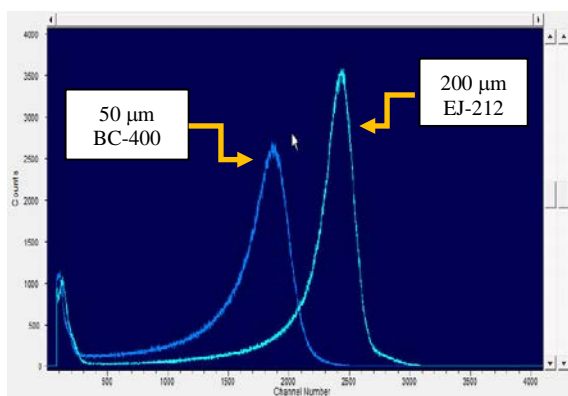
Fig. 8. Spectra induced from Pu-239 alpha peaks in 50 μm BC-400 and 200 μm EJ-212 plastic scintillator films. Pu-239 releases alpha particles of 3 different energy levels (5.105 MeV, 5.144 MeV, 5.156 MeV (11.5%, 15.1%, 73.3%)); hence, the peak has an asymmetric distribution in the left side of the peak.

Figure 9 shows that the total counts are stable throughout the range of the scintillator thickness as shown in blue plot; however, the peak centroid location shifts approximately 30% from 50 to 200 μm scintillators. This indicates that the full energy deposition occurs with more frequency at 200 μm even though the count rates increase by approximately 20%.
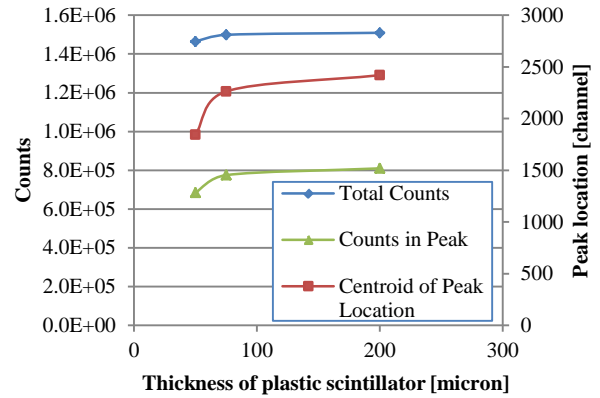
Fig. 9. Photon production responses of different plastic scintillator films. The total counts do not vary much among the thicknesses; however, the deposition of full energy varies as a function of the thickness, indicating that the full energy deposition may not be adequate at 75-micron thickness. The final selection of the scintillator thickness is deferred until the gamma response is observed.

Table I. Photon production responses of plastic scintillator films

Plastic Scintillator type	Total Counts (30 min)	Centroid of Peak Location (channel)	Counts in Peak
50 μm BC-400	1464759	1845	684784
75 μm BC-400	1498739	2263	775188
200 μm EJ-212	1509184	2420	809921

2.2. Scintillator Film: Gamma Sensitivity

Using the same methodology, gamma sensitivity of the plastic scintillator films was tested. Often, a neutron detector will operate in a gamma radiation field, and it's important to characterize the gamma sensitivity of the detector system to understand its capability. Fig. 10 shows the gamma measurement setup using a Cs-137 source. Using the same equipment as the Pu-239 alpha measurement, a Cs-137 source was placed 5 cm away from the scintillator film.

The spectra in Fig. 11 indicate a negligible difference between 50 and 75 micron scintillator films. However, Fig. 12 shows a noticeable difference between 50 and 200 micron scintillator films. There exists a peak in the spectrum for 200 micron film that didn't exist for other film thicknesses. Table II shows that the total counts for 50 and 75 micron film were less than 20% different, while the spectrum for 200 micron is more than twice the counts for the spectrum of the 50 micron

film. Therefore, 200 micron scintillator film was deemed too sensitive for gamma. This sensitivity will only increase as multiple layers of plastic scintillator films will be stacked in the prototype detector.
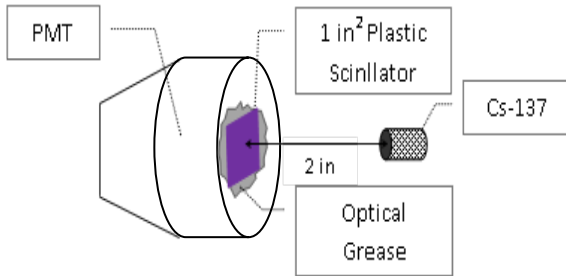
Fig. 10. The Gamma measurement setup using a Cs-137 source. One square-inch plastic scintillator piece was directly applied on to the PMT surface using optical grease. A Cs-137 source was placed 2-inch away from the PMT face for measurement.

Fig. 11 shows that the gamma induced pulses accumulate in the lower energy region, indicating that this is not a pileup issue. For both 50 and 75 micron film spectra, the higher energy regions beyond channel number 200 appear identical whereas the spectrum for 200 micron film in Fig. 12 shows that there is a peak.
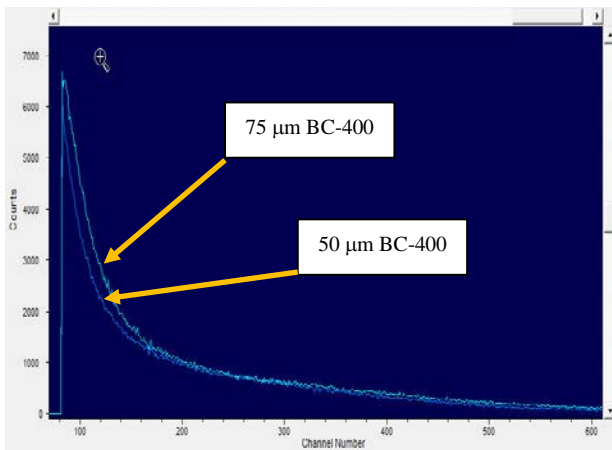
Fig. 11. The Cs-137 induced spectra for 50 and 75 micron thick plastic scintillator films. The spectra show similar response.
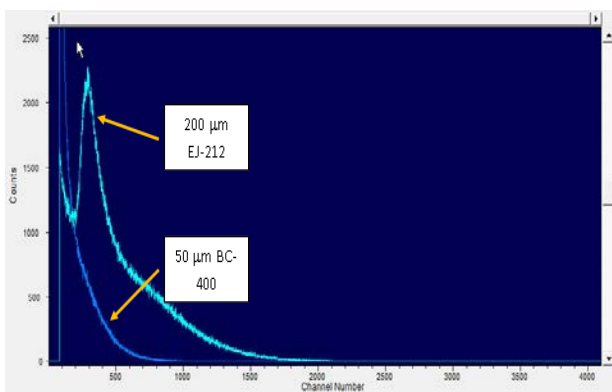
Fig. 12. The Cs-137 induced spectra for 200 micron film shows a peak indicating the film thickness is much more sensitive to the gamma contribution than other thinner films.

Table II. Gamma response of plastic scintillator films

Plastic Scintillator type	Total Counts (30 min)	Centroid of Peak Location (channel)	Counts in Peak
50 μm BC-400	417311	NA	NA
75 μm BC-400	495476	NA	NA
200 μm EJ-212	969659	310	670609

2.3. Scintillator Film: Combined Response

The gamma and alpha induced spectra for 200 micron scintillator film are juxtaposed in a one plot in Figs. 13 and 14. With a gamma induced peak near channel 400, the overlap between the gamma and alpha induced pulses is not trivial. The crossing over of the spectra occurs near the channel #1300. At higher channel numbers, the pulses induced by alpha particles dominates, while at lower channels gamma induced pulses dominates.
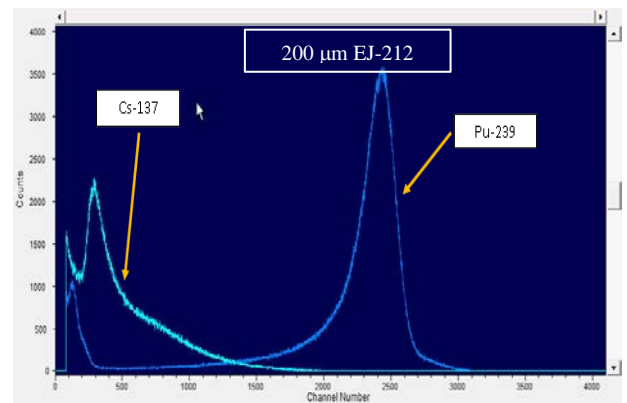
Fig. 13. Juxtaposition of Cs-137 and Pu-239 induced spectra for 200 micron EJ-212 film. The crossing over of the spectra occurs near the channel #1300. At channels higher than that, the response to alpha particles dominates, while at lower channels, gamma response is prominent.

On the other hand, the spectra for 50 micron scintillator film have a relatively wide separation between the gamma and alpha induced spectra and is less sensitive to gamma radiation as shown in Fig. 14. For this reason, 50 micron scintillator film was chosen as better suited material to detect neutrons in deployment with a gamma radiation field present.
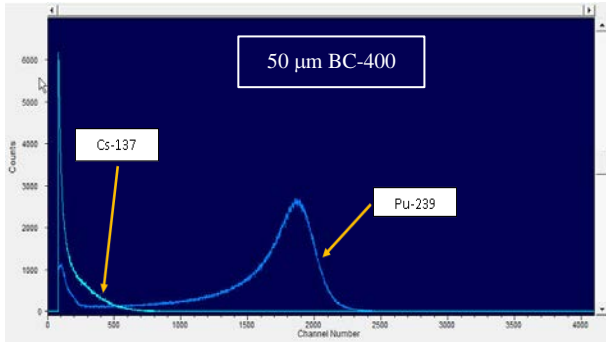
Fig. 14. Juxtaposition of gamma and alpha induced spectra for 50 micro BC-400 film. The cross over between Cs-137 and Pu-239 induced spectra occurs early at channel # 500.

3. Fabrication

The specification for the detector components was finalized and the components were procured. They were assembled in a dry room whose atmospheric moisture content was less than 2%. The light guide strips are laminated with 50 micron plastic scintillator film on both sides by Eljen Technology. The individual light guide strips are stacked with lithium foil in between. There are total 8 0.6mm thick light guide strips with 7 lithium foil inserted as shown in Fig. 15.

Fig. 15. The lithium foil pieces are cut and inserted between lightguides whose exterior surfaces are covered with plastic scintillator film.

The sandwich stack of laminated light guide strips and lithium foil is then inserted through 3 teflon holders, which are fastened with 4 threaded rods as shown in Fig. 16. The ends of the stack were coated with optical grease for optimal light transport through the interface.

Fig. 16. The sandwich stack of light guide, plastic scintillator, and lithium foil is assembled, ready for insertion into the hermetically sealed container.

The entire assembly was then inserted into a hermetically sealed enclosure. The enclosure, made with a 10 cm diameter stainless steel tube, was cut to the right

length and was welded to accept industry standard vacuum fittings.

Fig. 17. Insertion of the entire detector assembly into the hermetically sealed detector enclosure. The enclosure was filled with dry argon to prevent moisture leaking into the enclosure.

4. Characterization

Having been assembled and tested, the detector was shipped back the Los Alamos National Laboratory for characterization. Using gamma and fission neutron sources, the detector response was characterized.

4.1. Neutron Response

Figure 18 shows the epithermal neutron response of the detector. Initially, using a Cf-252 source, the detector registered 30% of the maximum count rate without the use of high density polyethylene (HDPE). The maximum count rate of 157 cps occurred with approximately 6 cm thick moderator as shown in Fig. 19. The sandwich configuration of the neutron conversion layers, even without the additional moderator on the outside, is sensitive to neutrons.

Fig. 18. Neutron response using a Cf-252 source. The measurement series started with no moderator material between the source and the detector that has been shielded with lead cylinder of 2 cm thickness.
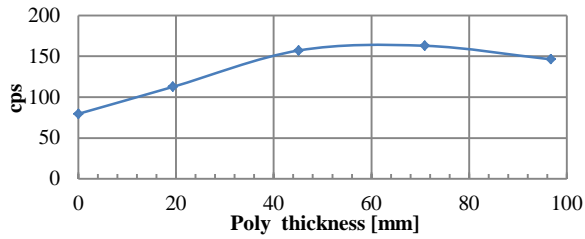
Fig. 19. Plot of the count rate as a function of moderator thickness. As moderator is added between the detector and the fission neutron source, the count rate increased until the maximum is achieved at approximately 6 cm of moderator thickness.

On another measurement series, the moderator thickness was increased on the back of the source to observe the contribution of the source neutrons backscattering to the detector after the initial direction. Again, without any moderator, the detector performed approximately 30% of the maximum count rate. The maximum count rate of 700 cps occurred after adding approximately 8 cm thick moderator.

Fig. 20. Another neutron measurement setup to observe epithermal neutron response of the detector. Moderator was added behind the neutron source to observe the contribution of the backscattering neutrons.
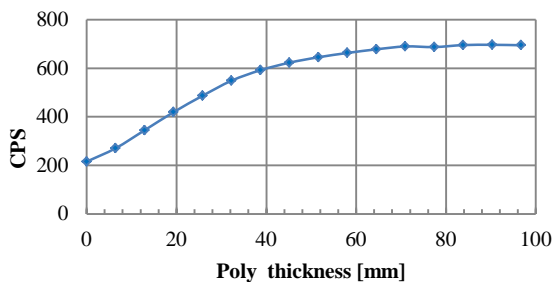
Fig. 21. A plot of detector response for epithermal neutrons. The maximum count rate occurs with a total 7 cmms thick HDPE backscattering neutrons.

4.2. Gamma Sensitivity

Using a Cs-137 source, a gamma induced spectrum was obtained. Using the same energy scale, a Cf-252 induced spectrum was obtained as shown in Fig. 22. An arbitrary division was made to exclude gamma induced and background pulses from the high energy region, where a pulse height discrimination method may be applied to minimize gamma contribution from the pulse

counts. By using this method, the lithium sandwich detector achieved 370 cps after subtracting background and gamma induced pulses when a helium-3 proportional counter with an active length of 22 inch registered 385 cps. This shows that the lithium sandwich detector performance is comparable to a similarly sized He-3 proportional counter, a de-facto standard of thermal neutron counting.
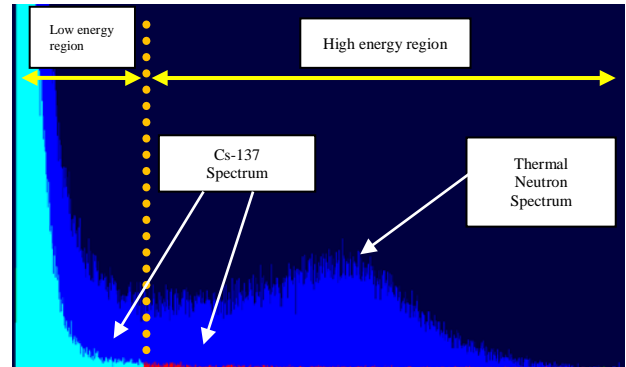
Fig. 22. Neutron and gamma induced spectra on the same arbitrary scale. Using the Cs-137 induced spectrum as the guide an arbitrary point was used to dive the scale into two regions, one low energy region and one high energy region. In the low energy region, there was a mixture of background, gamma, and neutron induced pulses, whereas in the high energy region, mostly neutron induced pulses were present.

Table III. Separation of gamma and neutron induced pulses for the lithium sandwich detector.

	Low Energy Region	High Energy Region
Back-ground	145	
Gamma-induced pulses	1100	60
Neutron-induced pulses	1770	1564

5. Conclusion

Starting with the material procurement and processing, steps taken to develop a novel neutron detector have been shown. The lithium foil detector has maintained the neutron capture ability by employing conventional off-the-shelf high vacuum components to keep atmospheric moisture from penetrating through the hermetically sealed enclosure. The sandwich detector shows comparable performance with a He-3 proportional counter. While the detector is under-moderated with this design, a future design shown in Fig. 23 will try to increase the detector efficiency by using a square PMT to cover the entire face. By electronically eliminating the gamma induced pulses from the majority of the neutron induced pulses, a simple pulse height discrimination technique may be sufficient to detect only neutron induced pulses in a mixed radiation field.

Using the lithium sandwich detector as a basic module, Fig. 24 shows a depiction of a multiplicity counter design made up of 8 modules. A preliminary calculation shows that the detector has a much shorter die-away time and dead time than existing multiplicity counters based on the He-3 proportional counter design. The prototype of this detector is being developed at the moment.
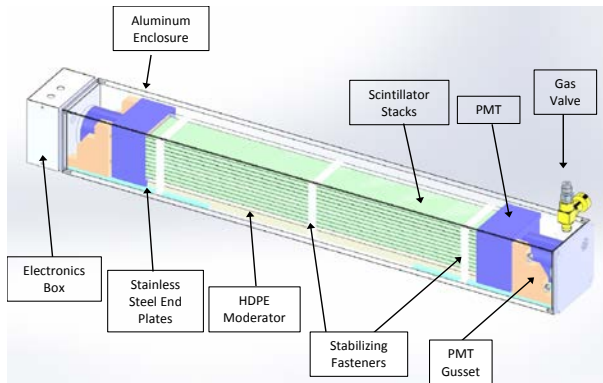
Fig. 23. A picture of a production model using a square PMT for a bigger lithium sandwich stack. It is expected that this optimization will increase detector efficiency.
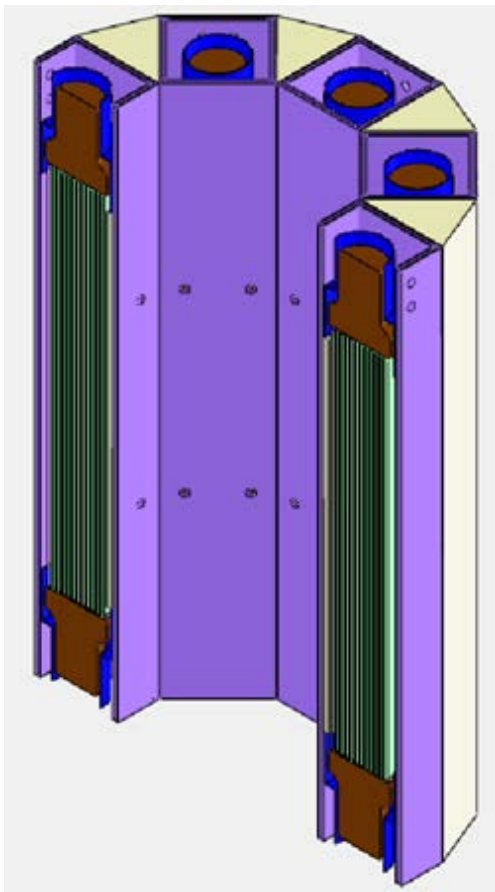
Fig. 24. A multiplicity detector diagram using 8 lithium sandwich detectors. It is expected that it would have a shorter die-away time, less dead-time, and higher detector efficiency than the ones based on He-3 proportional counters.

REFERENCES

[1] C. M. Lederer and V. S. Shirley, Table of Isotopes, 7th Ed., Wiley, 1978.
[2] G. F. Knoll, Radiation Detection and Measurement, Wiley, 2010.
[3] D. Shea, The Helium-3 Shortage: Supply, Demand, and Options for Congress, Congressional Research Service, 2010.
[4] United States Congress, Caught by Surprise: Causes and Consequences of the Helium-3 Supply Crisis. 2010.
[5] K. Chung, Design and Optimization of Lithium-6 Neutron-Capture Pulse-Mode Ion Chamber, dissertation, 2008.
[6] K. Chung, K. Ianakiev, M. Swinhoe, and M. Makela, Large-Area Neutron Detector Based on Li-6 Pulse Mode Ionization Chamber, Presented at the Institute of Nuclear Material Management, 46th Annual Meeting, 2005.
[7] K. Chung, K. Ianakiev, M. Swinhoe, and M. Makela Mitigation of Outgas Effects in the Neutron-capture Li-6 Pulse-Mode Ionization Chamber Operation, Presented at IEEE Nuclear Science Symposium, 2005.
[8] T. J. Gooding and H. G. Pugh, The Response of Plastic Scintillators to High-Energy Particles, Nuclear Instruments and Methods Vol. 7, pp 189-192, 1960.